Journal of The Electrochemical Society, **160** (4) A610-A615 (2013)
0013-4651/2013/160(4)/A610/6/$31.00 © The Electrochemical Society

In-Situ Measurement of Current Distribution in a Li-Ion Cell

Guangsheng Zhang,[a,*] Christian E. Shaffer,[b] Chao-Yang Wang,[a,b,*,z] and Christopher D. Rahn[a]

[a]*Electrochemical Engine Center (ECEC) and Department of Mechanical & Nuclear Engineering, The Pennsylvania State University, University Park, Pennsylvania 16802, USA*
[b]*EC Power, State College, Pennsylvania 16803, USA*

This paper reports in-situ measurements of current distribution in a Li-ion battery using a newly developed pouch cell with a segmented electrode. It is shown that current distribution is non-uniform from the beginning of discharge and evolves dramatically as discharge proceeds. Initially, segments closer to the negative tab generate higher local currents, which is attributed to the ohmic potential drop along the negative current collector. However, toward the end of discharge the current distribution reverses in pattern due to local SOC non-uniformity developed by uneven current production in early stages. Current distribution is more uniform at lower C rates and lower temperatures. In cells operated close to the equilibrium (e.g. at low C-rates or higher temperatures), current distribution tends to be wavy as it is dominated by the SOC non-uniformity effect and reflective of multiple plateaus in the open-circuit voltage vs. SOC curve. In contrast, current distribution exhibits a monotonic variation in cells operated at highly non-equilibrium as the ohmic potential drop along the current collector becomes more controlling. Local SOC distribution is calculated based on measured local currents. The SOC distribution is found not uniform, even at cutoff during high C rate discharge, suggesting strongly under-utilization of active materials.
 [DOI: 10.1149/2.046304jes]

Manuscript submitted December 21, 2012; revised manuscript received January 22, 2013. Published February 8, 2013.

With high energy density, low self-discharge and long cycle life, the Li-ion battery has become the dominant power source for man-portable electronics since its commercialization in early 1990s.[1] In recent years, its application in electric vehicles has been proliferated.[1,2] As compared to application in consumer electronics, the application of Li-ion battery in electric vehicles is much more demanding in terms of energy and power density, safety, durability and cost. Although much progress has been made, grand challenges remain.[3–6] In particular, how to unlock the potential of existing Li battery materials and to scale up Li-ion cells to 10-100 Ah sizes without substantial loss in performance, durability and safety remains a key technological challenge.

Large Li-ion batteries are critical for vehicle and grid energy storage that would enable a sustainable energy future. In large-format Li-ion batteries, especially cylindrical and prismatic ones in which electrodes, separators and current collectors are wound or multi-layered, the pathways of current (e.g. through foil current collectors) and heat (e.g. through multi-layer rolls from inside to outside) are typically not equal at different locations of electrodes. Through complex interactions among the local reaction current, state of charge (SOC) and temperature, non-uniform spatial distribution of these critical parameters is inevitable, especially during high C-rate operation. These non-uniform distributions will lead to under-utilization of active materials loaded in a large cell, thereby drastically reducing its energy density from the coin cell benchmark. Indeed, the modeling study of Zhao et al.[7] revealed, for the first time, a direct and significant correlation between cell energy density and the non-uniformity in current distribution, as well as a potential to gain as much as 45% in cell energy density through improving the current distribution in a large Li-ion cell. Of equal importance, non-uniform current distribution results in localized overcharge or overdischarge, compromising durability and safety of large batteries. Therefore, understanding how these critical parameters distribute under various design and operation conditions greatly aids development of energy denser, safer, and more durable Li-ion batteries.

In recent years, electrochemical modeling has been widely used in the research and development of Li-ion batteries to gain insight into internal processes, predict performance, optimize cell design and operation, and accelerate development of new concepts/strategies.[8–15] A critical element for exercising battery models is experimental validation. Due to the non-uniform distribution of those critical parameters in a large Li-ion battery, a multi-dimensional (multi-D) battery model needs to be validated against not only overall cell performance, but also against spatially resolved data.

Therefore, it is of great importance to experimentally measure such critical parameters as current density, temperature and SOC, in Li-ion batteries locally, in order to reveal insight about their distribution characteristics and to provide spatially resolved data for multi-D model validation. Considering that distribution of those parameters is transient in nature, in-situ measurement is desired.

Prior research on this important topic has been very limited. As an important indicator of Li-ion battery performance and aging, local SOC received relatively more attention. Maire et al.[16] developed an in-situ colorimetry method to map SOC distribution based on the fact that electrode materials change color upon lithium intercalation. They demonstrated the application of this method in an aged graphite electrode and observed highly non-uniform SOC distribution. Liu et al.[17] and Nanda et al.[18] respectively used X-ray micro-diffraction (μXRD) and micron-resolution Raman spectroscopy for ex-situ mapping of the SOC distribution, both in the through-plane and in-plane directions of electrodes. As a powerful and non-invasive imaging technique, neutron radiography has great potential for in-situ mapping of SOC in Li-ion batteries, and the application was demonstrated by Butler et al.[19] and Siegel et al.[20] As for local temperature measurement, Lee et al.[21] embedded two micro temperature sensors into a Li-ion battery and observed slightly higher internal temperature than surface temperature during 1 C charge/discharge. Forgez et al.[22] inserted a thermocouple into the center of a 26650 Li-ion battery cell by drilling to access the central hole of jelly roll. The temperature measured by the internal thermocouple was compared with that measured on the cell surface. Obvious temperature difference was observed during pulse charge/discharge at high C rate. Forgez et al.[22] also recorded surface temperatures with infrared thermography, which showed very slight temperature difference at different locations on the surface. By developing a small pouch cell with multiple working electrodes and multiple layers of separators, Ng et al.[23] demonstrated measurement of local current density across the thickness of electrode and observed non-uniform current distribution even at very low C rate (C/37 in their study).

While some progress has been made in experimentally observing the non-uniform distribution in SOC, temperature or current density in Li-ion batteries, most work remained qualitative or provided few measurement results. Some methods were restricted to surface measurement[16] or ex situ.[17,18] To date, in-situ spatially resolved experimental data that can be readily used for model validation remain elusive.

*Electrochemical Society Active Member.
zE-mail: cxw31@psu.edu

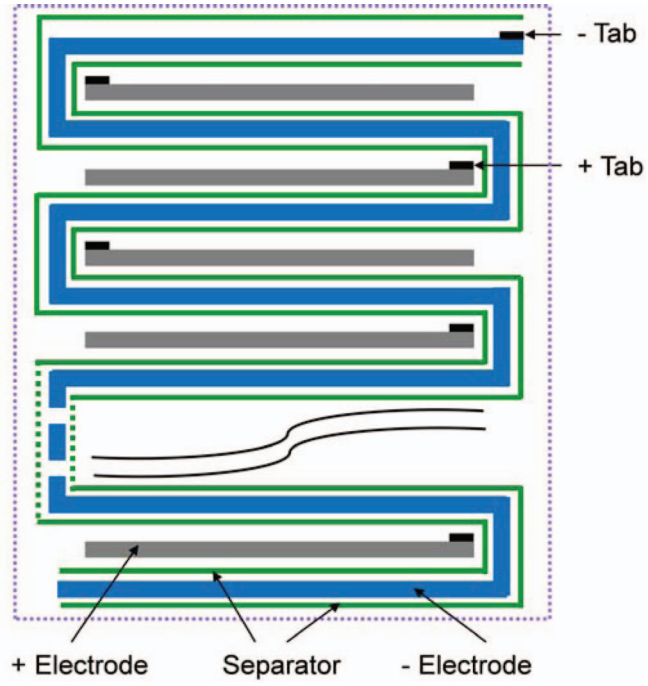

Figure 1. Schematic of the experimental pouch cell with a segmented positive electrode.

In this work, current distribution is measured in-situ along the length of an electrode sheet using a newly developed pouch cell with a segmented positive electrode. Current distribution under different discharge C rates and ambient temperatures is systematically investigated. Based on the current distribution data, information of SOC distribution during operation is also obtained. To our best knowledge, the present work is the first attempt to measure current distribution in-situ and provide spatially-resolved data for model validation.

Experimental

Experimental cell.— As schematically shown in Fig. 1, the experimental cell consists of one negative electrode (with active material coated on both sides of a Cu foil), two layers of separators, and multiple positive electrode segments (10 in this study, with active material coated on both sides of an Al foil). The negative electrode has one tab, which serves as the negative terminal of the cell, while every positive electrode segment has two tabs (with only one used in this study, as shown in Fig. 1). The negative electrode and separators are folded in a serpentine manner, with one positive electrode segment sandwiched inside each fold.

In the experimental cell, lithium iron phosphate (LFP) and graphite are used as positive and negative electrode materials. Celgard 2320 PP/PE/PP trilayer membrane (20 um thick)[24] is used as separator. The electrolyte is 1.2 M $LiPF_6$ in EC:EMC:PC (45:50:5 v%). The thickness of active material coating (each side) is 64 um in positive electrode and 43 um in negative electrode. The thickness of Al foil is 15 um and that of Cu foil is 10 um. Every positive electrode segment is 150 mm long and 56.5 mm wide (i.e. the coating area). The negative electrode is ~1.8 m long. Many more details of electrode fabrication are given elsewhere[25] and thus not repeated here. The electrode-separator sandwich is assembled in a pouch cell. After electrolyte filling, the pouch cell is sealed with one negative terminal and twenty positive terminals exposed to the outside.

Experimental system.— Fig. 2 shows a schematic of the experimental system in this work. Note that the segmented cell is unfolded and simplified here for convenience of understanding. The 10 positive electrode segments are connected in parallel to a bus wire, each through a shunt resistor (PLV7AL, 2 mΩ ± 0.5%, Precision Resistor Co., USA) for local current sensing. By connecting the 10 positive electrode segments in parallel and making resistance from the positive terminal bus to the Al tab uniform for each local channel, we can suppress the effects of Al foil on current distribution so as to focus on the effects of the negative Cu current collector. Such a configuration is also representative of a prevailing battery design with continuous tab along the positive electrode sheet (as the Al foil is more resistive) and discrete tabs on the negative electrode sheet (as the Cu foil is less resistive). A low resistance meter (3560, Hioki, Japan) is used to ensure that the resistance of shunt and connecting wires is the same for every channel (4.0 ± 0.1 mΩ in this study), and resistance of the bus wire is low enough to be negligible (<0.1 mΩ). The 4 mΩ resistance of shunt and connecting wires introduced for current measurements is negligibly small as compared to the internal resistance of each cell segment (~300 mΩ at room temperature).

A battery tester (BT2000, Arbin Instruments, USA) is used to control the overall current/voltage of the experimental cell. A multichannel data acquisition (DAQ) unit (34970A, Agilent Technologies, USA) is used to measure voltage drops across shunt resistors, which is then converted to local currents. Overall cell voltage is also recorded by the DAQ. All the data reported in this paper is recorded by the DAQ with a time interval of one second. To investigate the effect of the ambient temperature on current distribution, an environmental chamber (Tenney T10c, Thermal Product Solutions, USA) is used to control the ambient temperature during high- and low-temperature tests.

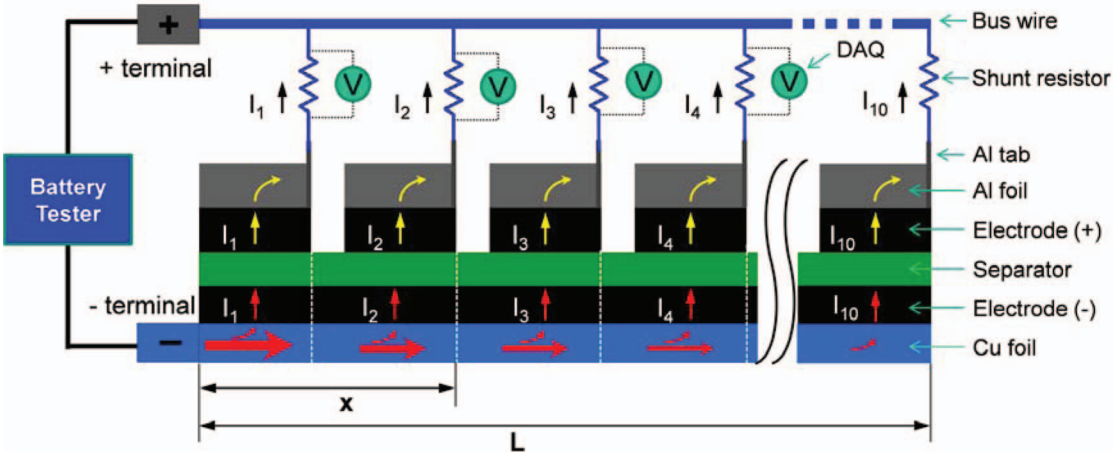

Figure 2. Schematic of the experimental system (cell unfolded and simplified; not to scale; arrows schematically showing current flow during discharge).

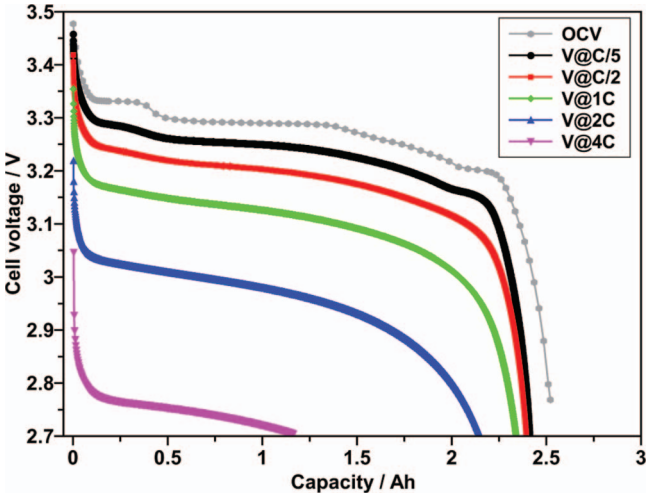

Figure 3. Cell performance at various discharge C rates at 21°C.

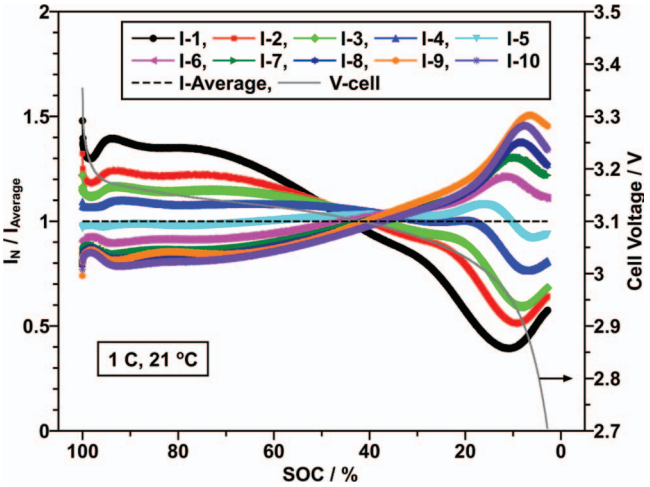

Figure 4. Local currents vs. cell state of charge (SOC) during 1 C discharge at 21°C.

Test procedures.— Before every test, the battery tester and DAQ are started and rested for one hour, then the cell is fully charged at room temperature (21°C) using a Constant Current-Constant Voltage (CC-CV) protocol (1.5 A, 3.6 V max, 0.05 A cutoff). Subsequently, the cell is rested for two hours (for test at 21°C) or four hours (for tests at 45°C and 0°C), allowing open circuit voltage (OCV) and temperature of the cell to reach equilibrium before discharge. For tests under different discharge conditions, the cell is discharged at specified C rate (based on nominal capacity of 2.4 Ah) until its voltage drops to 2.7 V.

Results and Discussion

Overall cell performance.— Fig. 3 shows overall performance of the experimental cell during discharge at various C rates (C/5, C/2, 1 C, 2 C and 4 C). The OCV performance is also shown, which is obtained by discharging the cell at C/10 intermittently with a rest period of one hour. As expected, the cell voltage and discharge capacity decrease with increasing C rate, which can be attributed to higher ohmic and kinetic overvoltage at higher current. The capacity at C/5 discharge is around 2.4 Ah, which is used as nominal capacity. The OCV variation matches open circuit potential (OCP, vs Li/Li^+) characteristics of LFP[26] and graphite[27] very well, suggesting the OCV variation is mainly from the OCP variation of graphite since LFP has a very flat OCP curve in a wide range.

Current distribution during 1 C discharge.— Fig. 4 shows the measured current distribution during 1 C discharge at 21°C. Note that local currents are made dimensionless after being normalized by the average current for convenient comparison among different cases. The discharge time is also made dimensionless for convenient comparison by using the cell SOC to indicate discharge progress. Average current (equal to the unity after normalization) and cell voltage are shown in the figure as reference. Fig. 5 shows dimensionless spatial distribution of local currents at different levels of cell SOC, using the local currents data extracted from Fig. 4. It can be seen clearly from these two figures that current distribution is not uniform from beginning of discharge and evolves significantly as discharge proceeds. Initially, segments closer to the negative terminal produce higher local currents than those farther away, i.e. $I_1 > I_2 > I_3 \ldots > I_{10}$. As discharge continues, local currents in segments with higher initial values generally decrease, while those with lower initial values increase, which leads to an entirely different pattern of current distribution near the end of discharge ($I_1 < I_2 < I_3 \ldots$). Note that I_9 is almost always slightly higher than I_{10} because segment 9 has slightly higher capacity than other segments (0.250 Ah vs 0.241 ± 0.004 Ah, obtained from integration of local currents in time during C/5 discharge).

The very non-uniform current distribution at the beginning of discharge can be attributed to the resistance of the negative current collector (10 um thick Cu foil, with resistance of ~55 mΩ for the whole length of 1.8 m). As schematically shown in Fig. 2, current flows in the Cu foil from the negative terminal to the other end, gradually decreases along the flow direction as local currents enter the negative electrode. As the current flows in, considerable potential drop along the Cu foil occurs due to its resistance. On the other hand, potentials of segments on the positive side (joint of shunt resistor with bus wire) are essentially equal due to negligible resistance of the bus wire. Consequently, the local overvoltage is smaller for segments farther from the negative terminal, thereby driving lower current according to electrochemical kinetics (e.g. Butler-Volmer Equation).[28] Therefore, the farther a segment is from the negative terminal, the smaller the local overvoltage is, and the lower current it generates. Higher SOC remains in regions far away from the negative terminal.

As discharge proceeds, the regions farther away from the negative terminal maintain higher SOC due to less current generation earlier and hence produce higher local currents. The dramatic variation of local currents during late stages of discharge can be attributed to the counteracting effects between potential drop along the Cu foil and the local SOC non-uniformity. The two effects counteract, tending to balance the current distribution. Therefore, local currents in segments

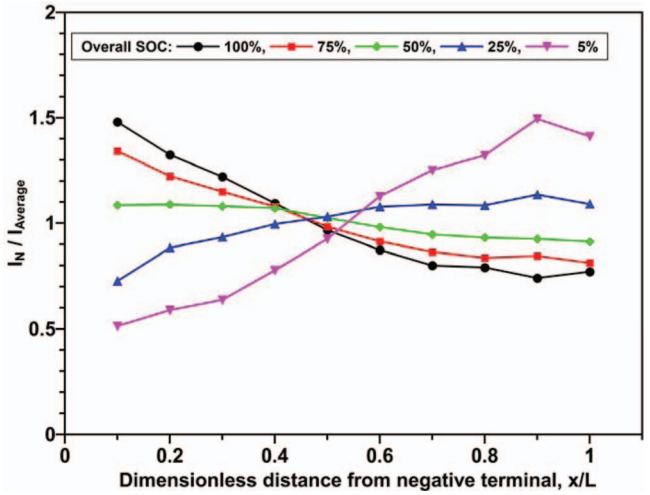

Figure 5. Spatial current distribution at different cell SOC during 1 C discharge at 21°C.

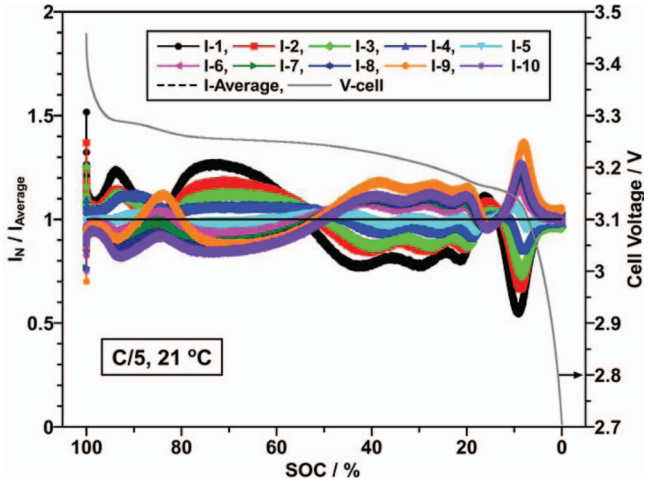

Figure 6. Local currents vs. cell SOC during C/5 discharge at 21°C.

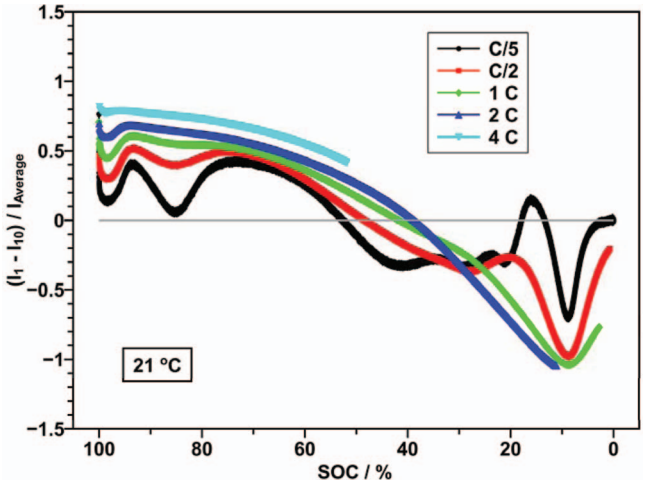

Figure 8. Maximum difference in local current during different C rate discharge at 21°C.

with higher initial values would decrease, while local currents in segments with lower initial values would increase. When the effect of local SOC non-uniformity overrides the effect of the ohmic potential drop along the Cu foil, in the case near the end of discharge, the current distribution would reverse in pattern, becoming entirely different from that at the beginning of discharge. See Figs. 4 and 5.

Effects of C rate on current distribution.— C rate is an important parameter for Li-ion battery operation, which influences both performance and durability, so current distribution in the experimental cell is measured at various C rates (C/5, C/2, 1 C, 2 C and 4 C) to investigate its effects. Results at C/5 and 4 C are shown in Fig. 6 and Fig. 7, respectively, for comparison with results at 1 C. It can be seen clearly that local currents spread less during lower C-rate discharge, indicating more uniform current distribution. This trend can be more clearly seen from Fig. 8, in which the differences between I_1 and I_{10} during different C rate discharge are plotted together. Segments 1 and 10 are most apart along the negative current collector, and I_1 and I_{10} are most different, so their difference, i.e. the maximum ΔI, can be used to represent the non-uniformity of current distribution in the experimental cell.

The effects of C-rate on current distribution again can be attributed to the opposing effects of potential drop along the Cu foil and the local SOC non-uniformity. During low C rate discharge (C/5), potential drop along the Cu foil is so small that the local current distribution is controlled by local SOC non-uniformity. Indeed a wavy pattern, evident from Figs. 6 and 8, results, reflective of multiple plateaus and frequent slope changes seen in the OCV vs. SOC curve. On the other hand, during high C rate discharge (4 C) the potential drop along the Cu foil, amounting to ~20 times larger than that during C/5 discharge, dominates the local current distribution. This dominance by the ohmic potential drop creates smoothly varying patterns, as can be seen clearly from Fig. 8 for the cases of 1 C, 2 C and 4 C. We hypothesize that a battery operated in close vicinity to the equilibrium features a wavy current distribution while a battery operated far away from the equilibrium would exhibit a monotonic variation.

Effects of ambient temperature on current distribution.— Ambient temperature is another important operating parameter for Li-ion batteries. Fig. 9 and Fig. 10 show the current distribution at elevated temperature (45°C) and lower temperature (0°C) during 1 C discharge. Comparison with the results at 21°C, as shown in Fig. 4, clearly indicates lower overall performance but more uniform current distribution at lower ambient temperature. This interesting phenomenon can be mainly attributed to the effects of temperature on the internal resistance of Li-ion battery cells, which includes the ohmic resistance (R_o), the charge transfer resistance (R_{ct}) and the resistance of SEI (R_{sei}). Previous studies[4,29] show that the charge transfer resistance and the SEI resistance increase dramatically at lower temperature while

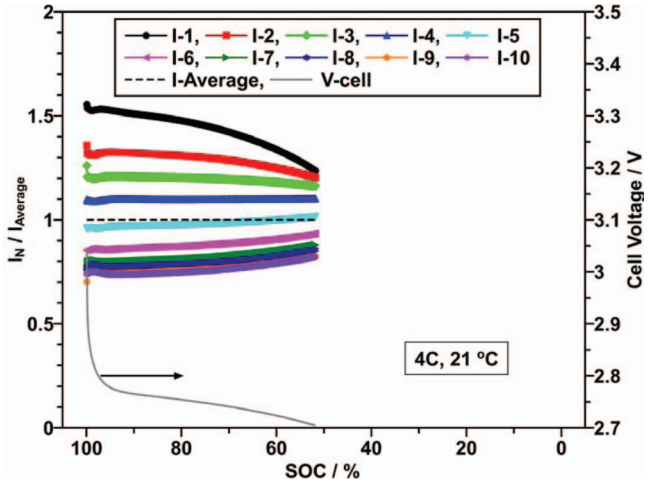

Figure 7. Local currents vs. cell SOC during 4 C discharge at 21°C.

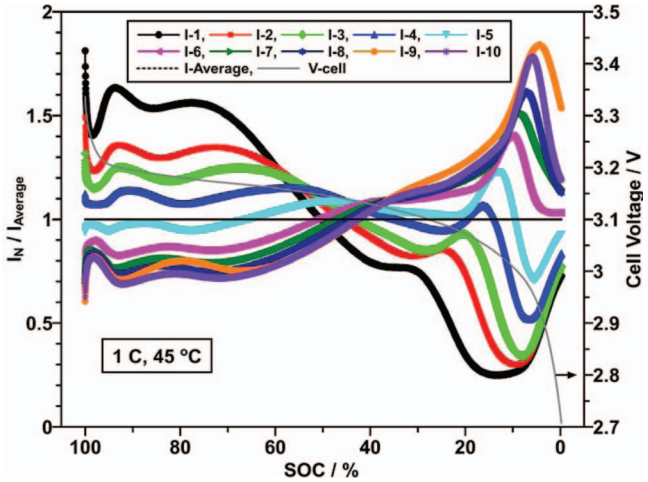

Figure 9. Local currents vs. cell SOC during 1 C discharge at 45°C.

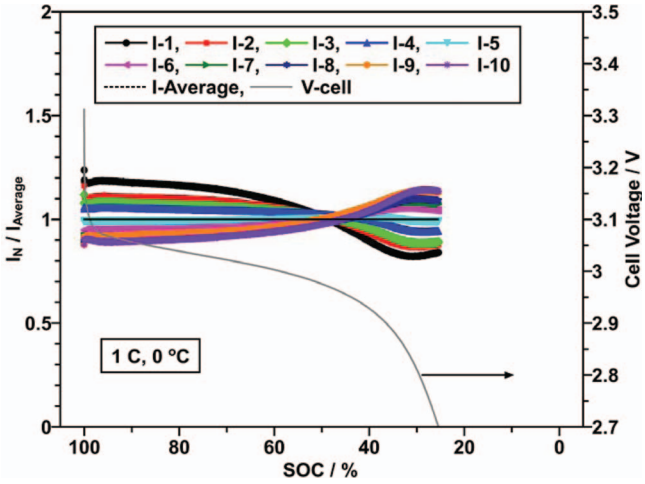

Figure 10. Local currents vs. cell SOC during 1 C discharge at 0°C.

the ohmic resistance change little. According to the previous studies, internal resistance of the experimental cell in this study would be much higher at 0°C in comparison with that at 21°C. As suggested in Fig. 2, higher charge transfer resistance and SEI resistance at lower temperature would make the effects of ohmic potential drop along the Cu foil less significant on the current distribution. Therefore, the current distribution would be more uniform at lower temperature. Obviously, higher internal resistance would reduce the overall performance of the experimental cell due to higher overvoltage at the same current. The better overall performance yet more non-uniform current distribution at 45°C agrees with the explanations as well.

Note that the resistance of Cu foil is slightly lower at lower temperatures (the temperature coefficient of Cu resistivity is $\sim 0.4\%^{\circ}C^{-1}$),[30] so the potential drop along the Cu foil is lower, which could also contribute to the more uniform current distribution at low temperatures. However, this effect is minor in comparison with the change of charge-transfer and SEI resistances with temperature.

Local SOC distribution.— With information on local currents, local SOC during discharge can be calculated, providing additional data for model validation. Discharged capacity of every segment can be calculated by integrating local current in time from beginning of discharge. Then local SOC can be obtained by taking capacity of local segment during C/5 discharge as reference of SOC = 100%.

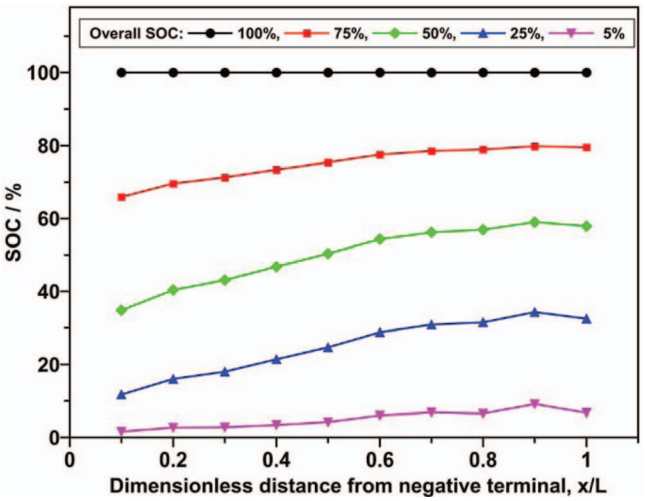

Figure 11. Local SOC distribution at different cell SOC during 1 C discharge at 21°C.

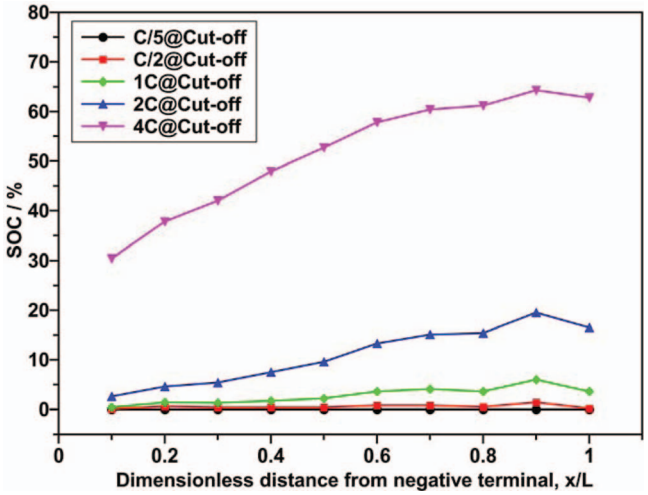

Figure 12. Local SOC distribution at cutoff during different C rate discharge at 21°C.

Fig. 11 shows distribution of local SOC at different cell SOC during 1 C discharge. As expected, the SOC distribution first becomes more and more non-uniform as discharge proceeds due to the higher local currents closer to the negative terminal, and then the SOC distribution becomes less non-uniform as discharge approaches end of discharge due to the reversal of current distribution.

It is interesting to note that the SOC distribution is still not uniform at cutoff for 1 C discharge. This phenomenon is even more obvious at higher C rates, as can be seen from Fig. 12, which shows SOC distribution at cutoff for different C rate discharge. For the 4 C discharge, local SOC of segment 1 is around 30%, while that of segment 10 is higher than 60%. Such highly non-uniform SOC distribution at cutoff significantly under-utilizes the active materials loaded in the battery, thereby reducing its energy density. Indeed, the very high SOC of segment 10 suggests that active materials in certain locations are largely under-utilized, a significant waste of battery materials.

Note that non-uniform SOC distribution at cutoff suggests non-uniform local OCV distribution, which causes internal balancing currents when the cell is placed on open circuit after cutoff. The internal balancing currents were indeed observed in our experiments and a detailed study on this topic is underway, which will be reported in a future publication.

Conclusions

Current distribution in a Li-ion battery is measured in-situ for the first time using a newly designed pouch cell with a segmented electrode sheet. Results show that current distribution is not uniform from the beginning of discharge and evolves dramatically as discharge proceeds. Initially, segments closer to the negative terminal have higher local currents due primarily to the ohmic potential drop along the negative current collector. On the contrary, near the end of discharge, current distribution reverses in pattern, attributed to the effect of local SOC non-uniformity. Effects of C rate and ambient temperature on current distribution are investigated. It is found that current distribution is more uniform at lower C rates and lower temperatures. The former can be attributed to lower potential drop along the current collector foil at lower C rate, and the latter can be mainly attributed to the cell's higher internal resistance at lower temperature. SOC distribution during discharge is also obtained based on the information on local currents. It is found that SOC distribution is uneven during discharge, even at cutoff during high C rate discharge, clearly indicating under-utilization of active materials.

Acknowledgments

The authors gratefully acknowledge funding from The United States Department of Energy (CAEBAT Program) through a subcontract from EC Power. The authors are also thankful to Dr. Yancheng Zhang for many valuable discussions and to EC Power for providing the segmented cell fixture used in this work.

References

1. J. Dahn and G. M. Ehrlich, Chapter 26 in *Linden's Handbook of Batteries*, 4th ed., T. B. Reddy and D. Linden, Editors, McGraw-Hill, New York (2010).
2. V. Etacheri, R. Marom, R. Elazari, G. Salitra, and D. Aurbach, *Energy Environ. Sci.*, **4**, 3243 (2011).
3. DOE, Fiscal Year 2011 Progress Report for Energy Storage R&D, http://www1.eere.energy.gov/vehiclesandfuels/resources/vt_es_fy11.html, (2012).
4. Y. Zhang and C. Y. Wang, *J. Electrochem. Soc.*, **156**, A527 (2009).
5. Y. Zhang, C. Y. Wang, and X. Tang, *J. Power Sources*, **196**, 1513 (2011).
6. K. Smith, T. Markel, G. H. Kim, and A. Pesaran, Design of Electric Drive Vehicle Batteries for Long Life and Low Cost, in *IEEE Workshop on Accelerated Stress Testing and Reliability (ASTR)*, Oct. 6-8, Denver, Colorado (2010).
7. W. Zhao, G. Luo, and C. Y. Wang, *Energy & Environ. Sci.*, submitted for publication (2013).
8. M. Doyle, T. F. Fuller, and J. Newman, *J. Electrochem. Soc.*, **140**, 1526 (1993).
9. K. Smith and C. Y. Wang, *J. Power Sources*, **160**, 662 (2006).
10. K. Smith and C. Y. Wang, *J. Power Sources*, **161**, 628 (2006).
11. V. Ramadesigan, R. N. Methekar, F. Latinwo, R. D. Braatz, and V. R. Subramanian, *J. Electrochem. Soc.*, **157**, A1328 (2010).
12. S. Santhanagopalan, Q. Guo, P. Ramadass, and R. E. White, *J. Power Sources*, **156**, 620 (2006).
13. V. Ramadesigan, P. W. C. Northrop, S. De, S. Santhanagopalan, R. D. Braatz, and V. R. Subramanian, *J. Electrochem. Soc.*, **159**, R31 (2012).
14. W. Fang, O. J. Kwon, and C. Y. Wang, *Int. J. Energy Res.*, **34**, 107 (2010).
15. G. Luo and C. Y. Wang, Chapter 7 in *Lithium-Ion Batteries*, X. Yuan, H. Liu, and J. Zhang, Editors, CRC Press (2012).
16. P. Maire, A. Evans, H. Kaiser, W. Scheifele, and P. Novak, *J. Electrochem. Soc.*, **155**, A862 (2008).
17. J. Liu, M. Kunz, K. Chen, N. Tamura, and T. J. Richardson, *J. Phys. Chem. Lett.*, **1**, 2120 (2010).
18. J. Nanda, J. Remillard, A. O'Neill, D. Bernardi, T. Ro, K. E. Nietering, J. Y. Go, and T. J. Miller, *Adv. Funct. Mater.*, **21**, 3282 (2011).
19. L. G. Butler, B. Schillinger, K. Ham, T. A. Dobbins, P. Liu, and J. J. Vajo, *Nucl. Instrum. Methods Phys. Res., Sect. A*, **651**, 320 (2011).
20. J. B. Siegel, X. Lin, A. G. Stefanopoulou, D. S. Hussey, D. L. Jacobson, and D. Gorsich, *J. Electrochem. Soc.*, **158**, A523 (2011).
21. C. Y. Lee, S. J. Lee, M. S. Tang, and P. C. Chen, *Sensors*, **11**, 9942 (2011).
22. C. Forgez, D. Vinh Do, G. Friedrich, M. Morcrette, and C. Delacourt, *J. Power Sources*, **195**, 2961 (2010).
23. S. H. Ng, F. La Mantia, and P. Novak, *Angew. Chem. Int. Ed.*, **48**, 528 (2009).
24. Celgard, Celgard High Performance Battery Separators, http://www.celgard.com/pdf/library/Celgard_Product_Comparison_10002.pdf, (2009).
25. J. Y. Eom, L. Cao, and C. Y. Wang, *J Power Sources*, *submitted for publication* (2013).
26. A. Yamada, H. Koizumi, S. I. Nishimura, N. Sonoyama, R. Kanno, M. Yonemura, T. Nakamura, and Y. Kobayashi, *Nat. Mater*, **5**, 357 (2006).
27. T. Ohzuku, Y. Iwakoshi, and K. Sawai, *J. Electrochem. Soc.*, **140**, 2490 (1993).
28. A. J. Bard and L. R. Faulkner, *Electrochemical Methods: Fundamentals and Applications*, 2nd ed., John Wiley & Sons, Inc., New York (2001).
29. L. Liao, P. Zuo, Y. Ma, X. Chen, Y. An, Y. Gao, and G. Yin, *Electrochim. Acta*, **60**, 269 (2012).
30. M. A. Laughton and D. F. Warne, *Electrical Engineer's Reference Book*, 16th ed., p. 1/29, Elsevier (2003).